THE AMERICAN SOCIETY OF MECHANICAL ENGINEERS
Three Park Avenue, New York, N.Y. 10016-5990

99-GT-427

FATIGUE FAILURES OF CENTRIFUGAL IMPELLER DISKS

Willem Jansen

Paul K. Fetfatsidis

Northern Research and Engineering Corporation, Woburn, MA

SUMMARY

An unusual centrifugal impeller disk failure has been encountered in one of the stages of a multistage air compressor. The failure occurred when a triangular piece of metal separated from the disk at the rim of the impeller disk. Stress analyses show that the steady hoop stresses at the rim were very low. Metallurgical observations indicate that the failure was caused by high cycle fatigue in cast 17-4 PH steel. A modal analysis shows that the failure can be explained by a resonance condition. The excitation of the backward rotating tangential nodal pattern by the stationary vaned diffusers just downstream of the impeller rim causes this resonance condition. Avoiding the resonance condition by changing the number of diffuser vanes has eliminated the failures.

BACKGROUND

Centrifugal compressors have an important place in industrial processes. Single stages must meet ever-growing increases in demand for higher pressure-ratio, operating range, efficiency and longevity. Consequently, we see more encroachments on stress limits and life expectancy of the rotating impeller wheel. These demands affect the stresses as follows:

- Higher pressure-ratio brings with it higher rotational speeds and higher centrifugal stresses with less tolerance for vibratory stresses.
- Wider operating range leads to the use of backward sloped blading with associated higher rotational speed for the same pressure ratio. Increased centrifugal blade bending causes high blade-root stresses near the outer part of the impeller.
- High efficiency requires the use of vaned diffusers downstream of the impeller. Vaned diffusers may reflect unsteady pressure waves back into the impeller that may generate high vibratory stresses under resonance conditions.
- Longevity with the possibility of increased erosion and corrosion requires the use of defect tolerant materials or reduction of allowable stresses.
- Eliminating shrouded impellers for open impellers with the associated question of clearance control.

In the following only open impeller wheels are considered.

CENTRIFUGAL IMPELLER FAILURES

One type of impeller failure is in the disk bore, where it is attached to a shaft. These failures are mainly due to high steady stresses imposed by the geometry of the disk, the extent of the rotating mass and the interference fit to the shaft. These failures are catastrophic and often result in uncontained rupture of the impeller.

A second type of failure is the development of cracks in the blades and the eventual separation of the blades from the impeller disk. These failures are usually contained, with damage restricted to the bearing system and internal casing. Blade cracks seldom occur due to high steady stresses alone. They mostly develop as a result of high vibratory stresses due to resonance conditions often combined with high steady stresses, erosion or corrosion. These cracks will occur at nodal points anywhere in the blades (root, mean, tip, inlet, or discharge). Actually, the crack's location is often a guide towards design improvements.

Engineers have recognized most of these events and it is a tribute to them that impeller failures have been reduced considerably. Whereas thirty years ago our organization was involved with new cases of turbomachinery HCF failures at least twice a month, currently these occurrences have reduced to roughly four per year. Nevertheless, with higher speeds we see new failures that previously went unobserved. One such occurrence is impeller rim disk failure.

Disk Tip Failures

The failures that were reported in the impellers occurred in the outer rim of the disk, where a triangular piece of metal separated from the disk. The triangular piece fit between two impeller blades. One side of the triangle is part of the rim; the other two sides are formed by cracks from the rim, converging to a single point below the rim. Figures 1a and 1b show the impeller with the failed disk section. (Two saw cuts are visible in anticipation of removing the small section.)

These failures are obviously not initiated by blade vibrations, but by phenomena, that generate high stresses in the disk. Visual observations showed no typical "beach" marks that might indicate without a doubt that the failure was caused by high cycle fatigue.

Presented at the International Gas Turbine & Aeroengine Congress & Exhibition
Indianapolis, Indiana — June 7–June 10, 1999

Fig. 1a View of Impeller Damage

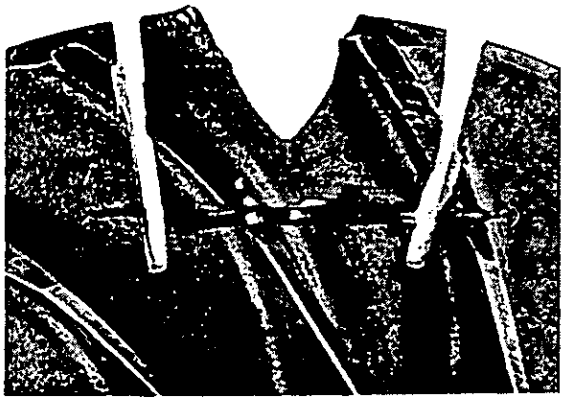

Fig. 1b Close-up View of Impeller Damage

Fractographic examination showed no casting defects at the origin of the crack. It is very unlikely that casting defects were present at the same location in all three failed impellers. For this reason, casting problems were eliminated as the cause of failure.

The impeller material is a high strength cast 17-4 PH stainless steel. This material has excellent yield strength but is not very tolerant to small defects. Small imperfections will grow rapidly under the influence of vibratory stresses. High hoop (tangential) stresses would cause a single crack near the middle of the passage between the blades, but calculated steady hoop stresses are around one tenth of the material yield strength. Low-cycle fatigue caused by infrequent stops and starts is hard to envision without any large steady stresses along the cracks.

The compressor shut down due to high bearing vibrations caused by

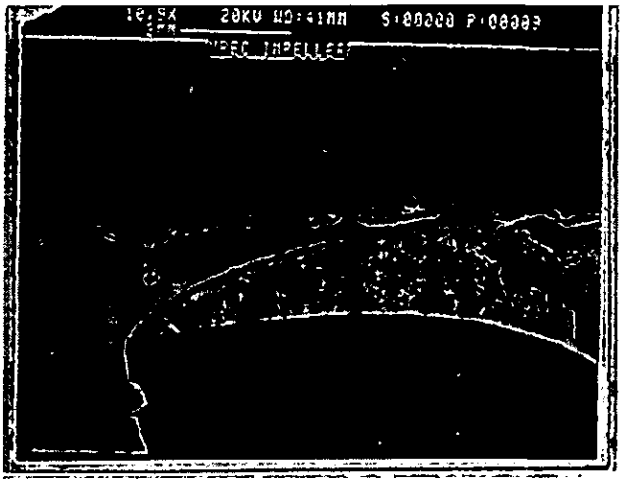

Fig. 2a SEM Micrograph of Fracture Face, Magn. 10.9X

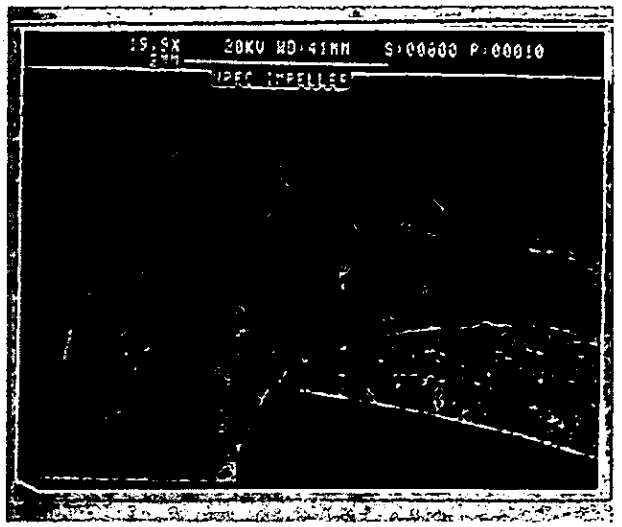

Fig. 2b SEM Micrograph of Fracture Face, Magn. 19.9X

the unbalanced impeller. No other area showed any cracks.

The cracks initiated on the bladed side and propagated towards the backface. The apex of the V-notch where the two cracks meet is shown in Figures 2a and 2b. These micrographs are taken with a Scanning Electron Beam Microscope. Fatigue striations are observed in the center at larger magnification (5000X). The spacing of these striations is around 0.6 microns. Analyzing the failure patterns shown in Figures 2a and 2b leads to the conclusion that the crack growth must have occurred along lines of high stress; this must be either a high tensile or a high vibratory stress at the nodal lines of an

excited natural frequency. As mentioned before, only the latter fits the pattern here.

The next important point to prove is that the failure is caused by resonance. If this can be proven then an impeller or vaned diffuser modification can be made that avoids the situation and prevents future failures.

There are two important elements to this proof:

1. Find the natural frequency of the mode that fits the failure. This means that the nodal lines of the mode of vibration should coincide with the failure cracks
2. Identify an excitation source that has the same frequency as the natural frequency of the failure mode.

Disk Vibrations

The analysis given here is relatively simple and serves mainly to illustrate the approach that was taken.

The impeller consists of a disk and blades that are attached to the

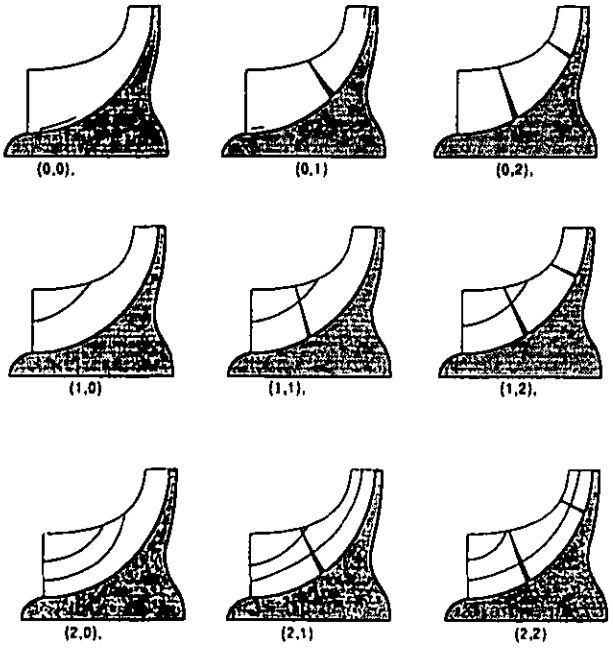

Fig. 3a Typical Impeller Blade Modes

disk. The blades themselves can have resonance problems and must be carefully designed to avoid these problems. The blades have so-called "flap" and lateral modes. These modes are indicated in Figure 3a. The disk has different natural frequencies of radial and tangential modes and combinations of these. These modes are shown in Figure 3b. These modes shapes charts are useful later to identify the modes found with the FEA analysis.

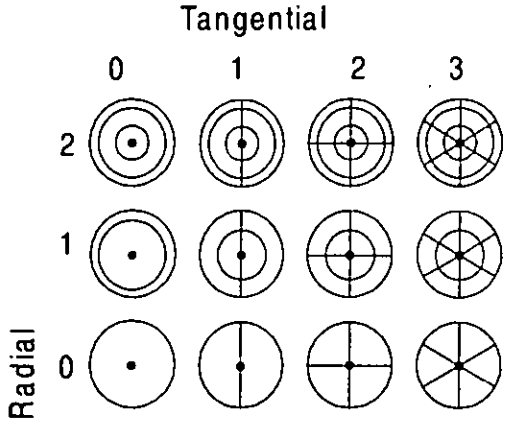

Fig. 3b Disk Nodal Patterns

For a disk at rest, the natural frequencies of these modes can be readily found through the application of FEA methods. However, a complication arises when the disk rotates. In that case, the vibration pattern starts to move around the circumference, both in the forward and backward direction. These phenomena are well known since the nineteenth century. The analysis was applied to large steam turbine disks by W. Campbell (1924), who explained their failures at a GE plant.

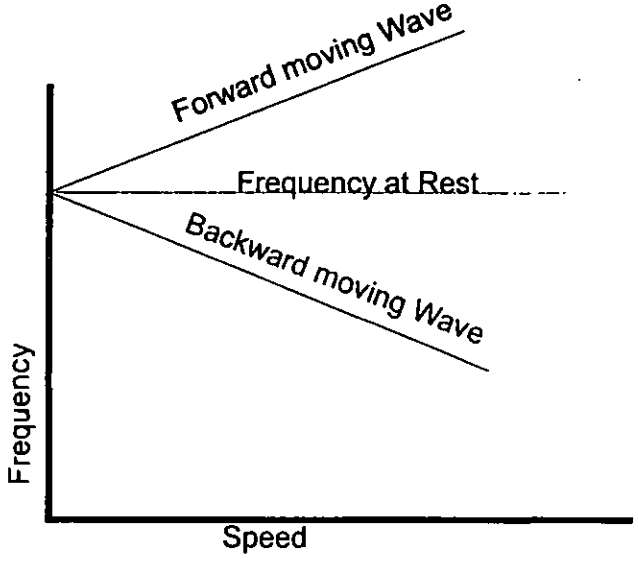

Fig. 4 Frequency shift caused by waves of nodal disk pattern as a function of running speed

Campbell found that when the disk is either at rest or rotating, the natural frequency of the disk vibrations did not change, except for the

centrifugal stiffening effect. This effect can be considerable for the lower modes but is very small for the higher modes. The stationary observer should be concerned about the rotation of the pattern. Campbell found that the forward moving waves are weak and do not cause failures. (This is in contrast to similar phenomena in rotor dynamics where both forward and backward running modes must be taken into account, Macke, 1966.)

Backward moving waves cause failures particularly when the speed of the waves reaches such a value that the vibration pattern becomes stationary. However, failures also occurred when the excitation coincided with the rotation of the pattern. The schematic in Figure 4 shows the effect of speed on frequency for a stationary observer under the influence of the forward and backward moving vibration pattern (waves). These phenomena are discussed in detail for the general case by Rao (1991) and for specific cases by Lalanne (1990).

The equations for finding the natural frequencies at rest are very complicated and are solved with FEA's for the disk at rest. However, when rotating the solution for the amplitude, Z, in axial direction takes the form of:

$$Z=\Sigma f(r,\theta)\, e^{(\omega t \pm \lambda\theta)}$$

where ω is complex, r indicates the radial and θ the tangential direction. The real value of ω indicates if the solution is stable or unstable while the imaginary part defines the frequency of vibration. The term, λ, a real number, is the wave number. The maximum amplitude of the wave varies with radius and circumferential direction, θ. It is a very complicated function, usually derived by assuming a series solution. The summation of the series and the functional relationship between r and θ is symbolized by $\Sigma f(r,\theta)$.

The tangential coordinate, θ, for a stationary observer can be expressed as $\theta = \Omega t$. That is, the radians that are traversed are a product of time and the disk speed in radians ($\Omega = 2\pi N/60$, where N is the disk rpm). ω is a negligible function of Ω, and thus we find that the wave speed, ω, for a stationary observer is:

$$\omega = \omega_R \pm \lambda\, \Omega$$

Or in terms of frequency:

$$f = f_R \pm \lambda\, N/60$$

where the subscript, R, refers to the disk at rest (N=0). Rejecting the forward running waves, the frequency for a stationary observer is then:

$$f = f_R - \lambda\, N/60$$

The speed of the backward wave is a function of the number of nodal patterns, λ, around the circumference times the speed in rps.

The resonance condition of the moving vibration pattern can be found similarly to the method used for blades and disks, namely through the interference diagram or Campbell diagram. This is shown in Figure 5. Campbell calls these interferences minor resonance speeds (as distinguished from major resonance speeds that occur when the traveling wave becomes stationary (i.e. $f_R = \lambda N/60$).

In the analysis, we searched for these disk resonance conditions. Particularly for resonances, which coincide with the nature of the cracks and the proximity of excitation forces such as those, generated by downstream vaned diffusers.

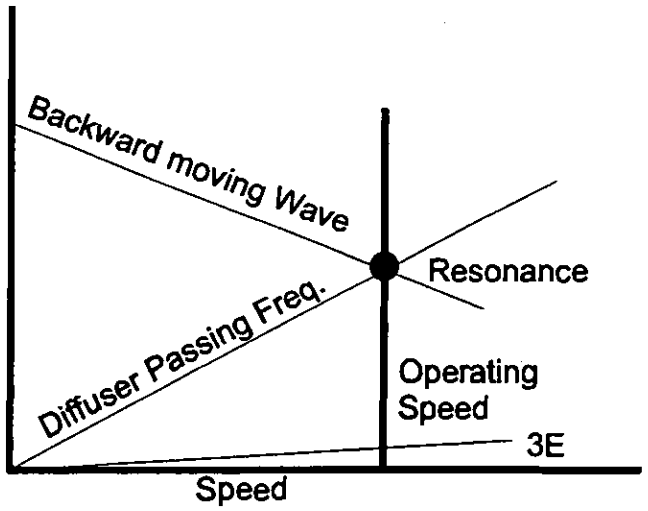

Fig. 5 Resonance pattern set up in rotating disk

FEA Modal Analysis of Impeller

The impeller has a tip diameter of 151 mm (5.95 inches), running at a design speed of 64,624 rpm. It has 16 blades and the inlet air temperature is around 44 deg C (110 F). The impeller material is non-coated and the fluid is well filtered before entering the stage. The impeller was part of a multistage air compressor with few stops and starts.

To avoid any ambiguities or the possibility of missing frequencies, a complete impeller model was prepared for analysis including all the sixteen impeller blades. The mesh model consisted of about 8,000 brick elements with grid fineness judiciously allocated to ensure accurate representation of the actual frequencies. A single layer of bricks was employed across the thickness of the blades. The discretization of the disk was governed by the necessity for matching nodes corresponding to the blade element nodal geometry. The disk section between adjacent blades was divided into two major segments, and subdivided further near the outer diameter. Thus, a basic 1/16 pie-cut was generated which could easily be modified for any parametric studies and could be copied/rotated to make a complete impeller model. For simplicity, the fillet at the blade root was omitted from the model since it was expected to have a relatively negligible effect on the results. Figure 6 shows a side view of the basic pie-cut solid model and grid used for the impeller.

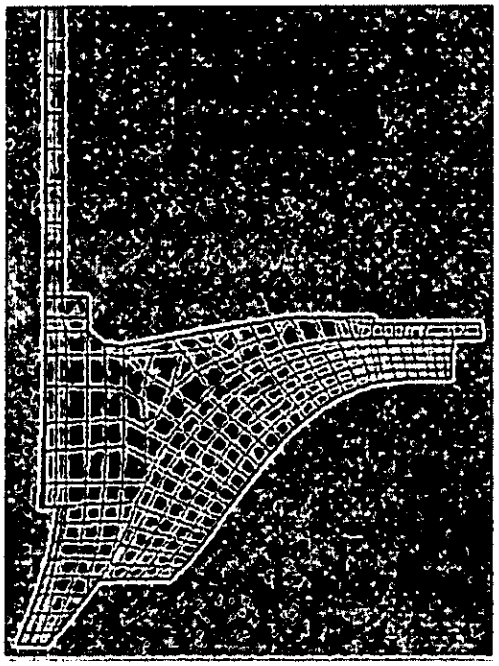

Fig. 6 FEA Grid used for finding blade and disk frequencies

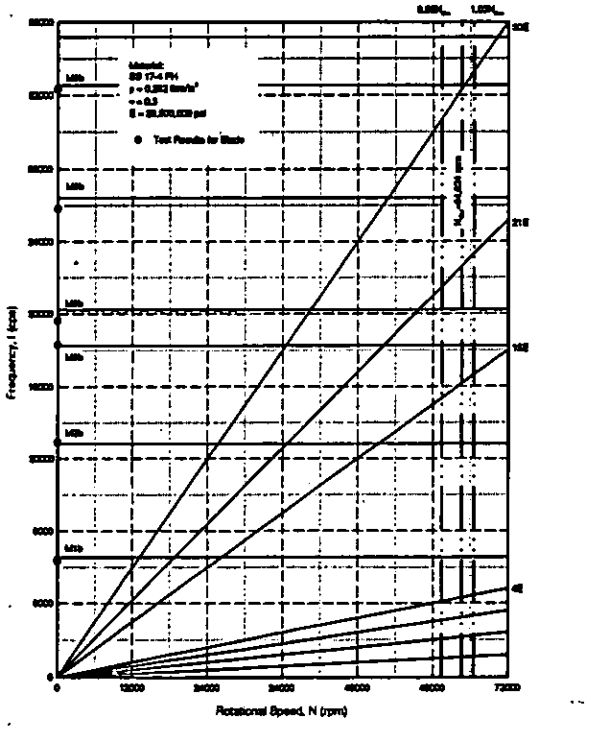

Fig. 7 Campbell Diagram for Impeller Blades only

Based on the shaft attachment, the applied boundary conditions were such as to constrain movement of all the nodes along the noted surfaces.

FEA Program, ANSYS, was used to calculate the frequencies of the impeller. The calculations were done for frequencies much higher than the required range to ensure best accuracy within the required range. The results were then imported to a graphics program to plot the Campbell diagram.

In order to assess the effect of a flexible disk, the frequencies were first calculated for a single blade fixed at the root (assuming a rigid disk), and subsequently for the complete impeller. The Campbell diagram for the single blade is shown in Figure 7.

Multiple Blade Modes

When the blades are considered fixed at the root in the disk, there is only one frequency at which the blades may vibrate. However, when the disk is somewhat flexible and the roots are part of the disk structure so that the blades can communicate with each other, there are many blade frequencies that can be excited.

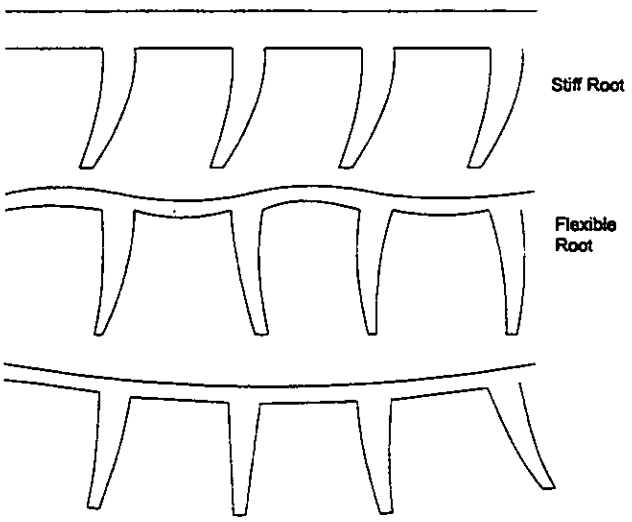

Fig. 8 Blade frequency influenced by flexible disk. Upper diagram shows blade root fixed. Blades only vibrate at one frequency. Two lower diagrams show some of the many interactions between disk and blade, yielding different blade natural frequencies with blades vibrating out-of-phase.

These frequencies are close together but the blades vibrate in different phases, subject to the flexibility of the disk at the root. Figure 8 shows the nature of this phenomenon. (It is well known in axial turbines, particularly when the blades have flexible shrouds that connect the blade tips).

The FEA analysis will yield the values of these multiple frequencies, provided the program is run for the entire disk and not just a pie-shaped sector.

Figure 9 shows the Campbell diagram with the frequencies calculated for the combined impeller blades and disk. The dark bands of frequencies represent various bending, longitudinal or torsional blade modes. Table 1 contains a listing of the frequencies as given by the ANSYS FEA program and the associated measured frequencies. . To give a basic understanding of the way the impeller structure vibrates, some selected blade and disk modes were identified and labeled relative to the convention shown in Figures 3a and 3b.

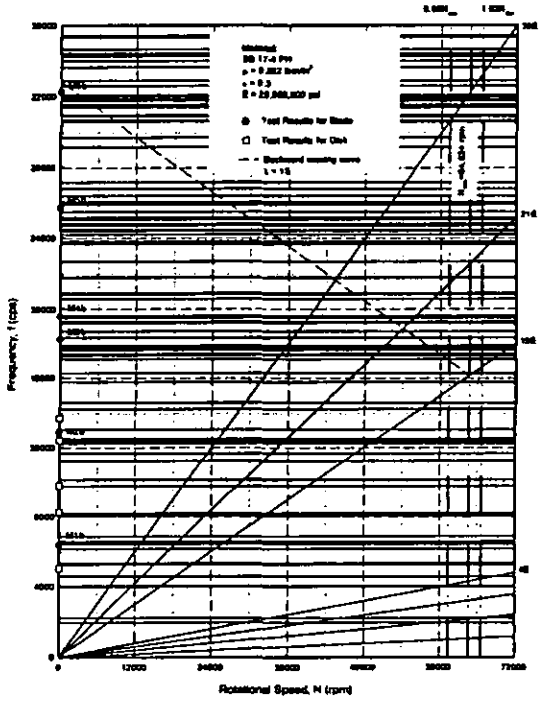

Fig. 9 Campbell diagram for impeller and disk

The only excitation sources are the diffuser vanes that can project slight pulses back into the impeller. The interactions between vaned diffusers and impellers have received considerable attention recently. Jin, et al. (1995) discuss the influence of vaned diffusers on impeller blade vibrations. Sanders, et al. (1998) measure the aerodynamic forcing functions of the vanes on impeller loading. In each of these cases the effects are reported worse when operating near the surge line and when the distance between the vanes and the impeller is small. In the current case the vaned diffuser leading edge is located at a radius ratio of 1.10 from the impeller tip. The disk rim is, however, closer to the vaned diffuser at a radius ratio of roughly 1.05 (see Figure 6).

The diffuser vanes only excite disk modes that have exactly the same diametral nodes as the number of vanes. No resonances will occur at dissimilar values. Since there are 15 vanes, we concentrate on the 15 nodal disk pattern. The frequency of the 15th nodal vibration pattern as calculated at rest is 32,852 Hz. Since the centrifugal stiffening for the 15th mode is slight, it is assumed that this frequency remains constant at speed. The operating speed is 64,624 rpm. The frequency of the backward wave pattern at the design speed is less than the frequency at rest by a value of 15 x 64,624 / 60, or 16,156 Hz. The frequency of the rotating wave pattern is then 32,852 - 16,156 or 16,696 Hz. Also, the excitation frequency of the diffuser vanes is 15 x 64,624 / 60 or 16,156 Hz. The backward wave is indicated in Figure 9.

This shows that the excitation frequency is within 3 percent of the 15th nodal disk frequency. In addition, the failure pattern fits the nodal line pattern of the 15 diametric nodes as shown in Figure 10. (The figure caption describes the nodal pattern and shows deformations based on "UZ" (axial) direction as determined by ANSYS.) Thus, it is concluded that the failure is a result of a resonance condition between the disk mode and the diffuser vanes.

Fig. 10 Impeller disk vibration pattern for 15 nodal diameters. Note: there are 16 impeller blades

Table 1 – Calculated and Measured Frequencies for the Impeller

SET	Frequency	Radial Mode, Nr	Tangential Mode, N8
1	1927	0	0
2	2189	0	1
3	2189	0	1
4	4001	0	2
5	4001	0	2
6	4009		
7	4550	0	3
8	4550	0	3
	5050	disk, measured	
9	5248		
10	5248		
11	5301	0	4
12	5301	0	4
13	6129	*	
14	6129	*	
	6375	M1b, measured	
15	6383	*	
16	6383	*	
17	6425	*	
18	6425	*	
19	6434	*	
20	6449	*	
21	6448	*	
22	6459	M1b, In-Phase (0,0)	
23	6496	*	
24	6496	*	
25	6512	*	
26	6512	*	
27	6570	*	
28	6570	*	
29	6855	0	5
30	6855	0	5
31	8038	0	6
32	8038	0	6
33	8172		
34	8172		
	8300	disk, measured	
35	8725	0	7
36	8725	0	7
	9800	disk, measured	
37	10109		
38	11202	0	8
39	11813	1	2
40	11913	1	2
41	12207	*	
42	12207	*	
43	12237	*	
44	12286	M2b, In-Phase (0,1)	
45	12312	*	
46	12312	*	
47	12350	*	
48	12350	*	
	12400	disk, measured	
49	12409	*	
50	12409	*	
51	12461	*	
52	12461	*	
53	12483	*	
54	12483	*	
55	12488	*	
56	12489	*	
	12925	M2b, measured	
57	13037	0	8
	13700	disk, measured	
58	14206	1	3
59	14206	1	3
60	14569	0	9
61	14569	0	9
62	15752		
63	15752		
64	16236		
65	16243	1	4
66	16243	1	4
67	17075	0	10
68	17075	0	10
69	17249	*	
70	17249	*	
71	17370	*	
72	17370	*	
73	17396	*	
74	17396	*	
75	17590	*	
76	17590	*	
77	17697	*	
78	17697	*	
79	17704	*	
80	17704	*	
81	17717	*	
82	17870	*	
83	17870	*	
	18300	M3b, measured	
84	18333	M3b, In-Phase (0,2)	
85	18693	*	
86	18693	*	
87	18163	M4b, In-Phase (1,1)	
88	19242	*	
89	19242	*	
90	19249	*	
91	19248	*	
92	19434	*	
93	19434	*	
94	19505	*	
95	18505	*	
96	19544	*	
97	19544	*	
98	18556	*	
99	19558	*	
100	19571	*	
	19600	M4b, measured	
101	19901	*	
102	19901	*	
103	20538		
104	20538		
105	20780		
106	20790		
107	20878	0	11
108	20878	0	11
109	21765	1	6
110	21765	1	6
111	22655		
112	23623	0	12
113	23623	0	12
114	23718	1	7
115	23716	1	7
116	23787	*	
117	23787	*	
118	24165		
119	24367	*	
120	24367	*	
121	24450	*	
122	24667	*	
123	24667	*	
124	24824	*	
125	24824	*	
126	25019	*	
127	25019	*	
128	25185	*	
129	25185	*	
130	25495	*	
131	25495	*	
	25800	M5b, measured	
132	25943	*	
133	25943	*	
134	26084	1	8
135	26437	0	13
136	26437	0	13
137	26830	M5b, In-Phase (0,4)	
138	26845	*	
139	26845	*	
140	27164	*	
141	27184	*	
142	29152	*	
143	29152	*	
144	29700	*	
145	30598	*	
146	30598	*	
147	30658	2	4
148	30656	2	4
149	30661	*	
150	30661	*	
151	30890	*	
152	30890	*	
153	30971	*	
154	30971	*	
155	31392	*	
156	31392	*	
157	31412	*	
158	31412	*	
159	31486	M6b, In-Phase (1,3)	
160	31469		
161	31468		
162	31500		
163	31500		
164	31553	*	
165	31565	*	
166	31565	*	
167	31757	0	14
168	31757	0	14
169	31841	*	
170	31841	*	
171	31982	*	
172	31982	*	
173	31983	*	
174	31983	*	
175	32084	*	
176	32084	*	
	32300	M6b, measured	
177	32560		
178	32852	0	15
179	32852	0	15
180	33613		
181	33955		
182	33955		
183	34220		
184	34220		
185	34351		
186	34394		
187	34394		
188	34616		
189	34618		
190	35286		
191	35288		
192	35300		
193	35300		
194	35429		
195	35420		

* Band of calculated blade frequencies that are Out-of-Phase, M#b denotes blade mode number

EXPERIMENTAL RING TEST OF IMPELLER

The purpose of the ringing test is to verify the accuracy of the calculated frequencies. A modal test of the natural frequencies and response for the impeller was carried out with the impeller installed in a specifically designed fixture. The test was conducted by ringing the blades with a sensitized hammer. The blade response was picked up by a condenser microphone and the signal processed with a Fourier analyzer. The blade frequency response is shown in Figure 11 for frequencies up to 40,000 Hz. Most of the responses are associated with the blade frequencies and show good correlation with the calculated results given in Figure 7. We did not take data for the higher disk modes.

However, Wachter, et al. (1983) show fairly good correlation between calculated and tested results for stationary impeller disk, particularly for the higher modes. Thus we are confident that the calculated disk modes are close to the actual values.

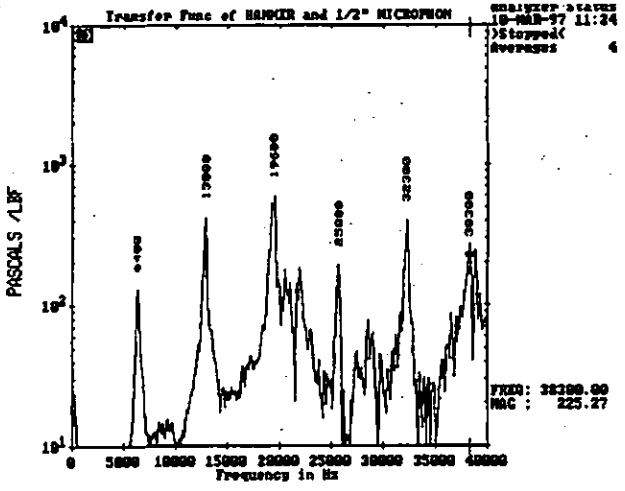

Fig. 11 Response of impeller to ring tests with pick-up close to the blades

Future Failure Avoidance

Having identified the failure mode, the recurring failures can be avoided by two means:

1. Change the disk natural frequencies. While this option is the most obvious, it is most expensive to accomplish. Making a new impeller casting or machining a new impeller is not inexpensive. In addition, a disk thickness change brings with it a change in weight and polar moment, with subsequent changes in rotor dynamics. It was found that a 50 percent increase in disk thickness increased the 15th diametral node by roughly 30 percent.
2. Eliminate the excitation mechanism. This change is readily made and the final number of diffuser vanes was set at 21.

The modified compressor stage was installed and has been running without failure for some three years.

ACKNOWLEDGEMENTS

The metallurgical work was conducted by Altran Materials Systems, Inc., while the ring tests were conducted by Strong Technology Co.

REFERENCES

Campbell, Wilfred, 1924. "The Protection of Steam Turbine Disk Wheels from Axial Vibration." *ASME Paper No. 1920.* Presented at the Spring Meeting, Cleveland Ohio, May 26 to 29, 1924

Jin, D., Jiang, Z., Hasemann, H., Haupt, U. and Rautenberg, M., 1995. "Influence of Vaned Diffuser on Dangerous Blade Vibrations due to Blade-Flow Interactions in a Centrifugal Compressor." *ASME Paper No. 95-GT-122.* Presented at the ASME IGTI Annual Conference, Houston TX, June 1995.

Lalanne, Michel and Ferraris, Guy, 1990. "Rotordynamics Prediction in Engineering." John Wiley and Sons.

Macke, H. J., 1966. "Traveling-Wave Vibrations of Gas Turbine Engine Shells." *Transactions of the ASME, Journal of Engineering for Power.* April 1966.

Rao, J. S., 1991. "Turbomachine Blade Vibrations." John Wiley and Sons

Sanders, A. J. and Fleeter, S, 1998. "Potential Field Interactions in a Low-Speed Centrifugal Compressor." *Journal of Propulsion and Power, Vol. 14, No. 6, November 1998.*

Wachter, J. and Celikbudak, H., 1983. "Vibration Analysis of Radial Compressor Impellers." *ASME Paper No 83-GT-156.* Presented at the ASME IGTI Annual Conference, Phoenix AZ, March 1983.